Galaxy-group-associated distances to Very High Energy gamma-ray emitting BL Lacs KUV 00311-1938 and S2 0109+22

Karri I. I. Koljonen[ID],[1,2,3]★ Elina Lindfors[ID],[2,4]† Kari Nilsson,[2] Pekka Heinämäki,[5] Jari Kotilainen[2,4]

[1]*Department of Physics, Norwegian University of Science and Technology, NO-7491 Trondheim, Norway*
[2]*Finnish Centre for Astronomy with ESO (FINCA), University of Turku, Väisäläntie 20, 21500 Piikkiö, Finland*
[3]*Aalto University Metsähovi Radio Observatory, PO Box 13000, FI-00076 Aalto, Finland*
[4]*Department of Physics and Astronomy, Vesilinnantie 5, University of Turku, 20014 Turku, Finland*
[5]*Tuorla Observatory, Department of Physics and Astronomy, Vesilinnantie 5, University of Turku, 20014 Turku, Finland*

ABSTRACT

Blazars constitute the most numerous source class in the known extragalactic population of very high energy (VHE) gamma-ray sources. However, determining their redshifts is often challenging due to weak or non-existent emission lines in their spectra. This study focuses on two BL Lacs, KUV 00311-1938 and S2 0109+22, where previous attempts at redshift determination have faced difficulties. By combining spectroscopic observations with photometric redshift estimates, we tentatively assign a redshift of $z = 0.634$ to KUV 00311-1938 and a likely redshift of $z = 0.49$ to S2 0109+22. Establishing redshift estimates for high-redshift blazars is crucial for understanding extragalactic VHE gamma-ray sources and their interactions with the surrounding universe.

Key words: galaxies: BL Lacertae objects: general – galaxies: distances and redshifts – galaxies: groups: general

1 INTRODUCTION

The number of known extragalactic very high energy (VHE) gamma-ray sources, with photon energies above 100 GeV, has increased from 10 to approximately 100 in the last 15 years, a trend anticipated to accelerate with the advent of the Cherenkov Telescope Array (CTA)[1]. These sources are predominantly blazars, a subset of Active Galactic Nuclei (AGN) characterized by a relativistic jet aligned closely with our line of sight. Consequently, the jet's emission experiences strong Doppler boosting.

Nearly 80% of the VHE gamma-ray-detected blazars belong to a group called BL Lacertae objects (BL Lacs), characterized by intrinsically weak optical emission lines likely resulting from a radiatively inefficient accretion flow toward the central supermassive black hole (Rees et al. 1982). Determining their redshifts through spectroscopy is particularly challenging due to the absence of emission lines that are overshadowed by the non-thermal continuum obscuring host galaxy features. However, fairly accurate redshift estimates can still be obtained based on absorption lines/edges of the H I Lyman α forest (e.g. Danforth et al. 2010; Dorigo Jones et al. 2022), redshift lower limits from intervening absorption systems (e.g. Furniss et al. 2013; Pita et al. 2014), and host galaxy CO lines in the millimeter regime (Fumagalli et al. 2012), which do not depend on the power of the non-thermal continuum. Nevertheless, many BL Lacs (~18%) still lack confirmed redshifts, despite numerous major observing programs targeting this abundant extragalactic VHE gamma-ray source population (e.g. Paiano et al. 2020; Goldoni et al. 2021; Kasai et al.

2023). Moreover, the leading candidate source of astrophysical neutrinos, TXS 0506+056 (IceCube Collaboration et al. 2018), is a BL Lac object with weak spectral lines (Paiano et al. 2017), further emphasizing the need for redshift determination efforts (Paiano et al. 2021).

BL Lacs, as bright extragalactic sources, provide valuable insights into the region of the universe between us and the blazar. VHE gamma-rays are absorbed through interactions with near- and mid-infrared photons of the extragalactic background light (EBL) that permeates the universe. This absorption is energy-dependent and becomes more pronounced with increasing redshift. Prior to modeling the VHE emission of blazars, this distortion must be corrected, requiring knowledge of the redshift of the source. Conversely, if the intrinsic blazar spectrum is known, VHE observations can be used to constrain the EBL in the infrared-UV bands. Thus, blazars at different redshifts can serve as indicators of the EBL density at varying wavelengths. The most recent limit, provided by Acciari et al. (2019) based on results from 32 gamma-ray spectra for 12 blazars within the redshift range of $z = 0.03 - 0.944$, is consistent with predictions from current EBL models. While the CTA has the potential to enhance these limits (Abdalla et al. 2021), achieving this goal requires an increase in the number of blazars with known redshifts, particularly those with $z > 0.4$, for which we currently have only ten sources[2]. In addition to studying the EBL, X-ray bright BL Lacs can also be utilized to investigate the warm-hot intergalactic medium (WHIM, $\log T(K) = 5 - 7$; e.g. Fang et al. 2007).

In this study, we aim to determine the redshifts of two BL Lacs: KUV 00311-1938 and S2 0109+22. Direct spectroscopic redshift determinations for these sources have proven challenging, and they

★ E-mail: karri.koljonen@ntnu.no
† E-mail: elina.lindfors@utu.fi
[1] https://www.cta-observatory.org

[2] see e.g. http://tevcat.uchicago.edu/

are likely to be located within a redshift range where blazars are scarce for indirect EBL studies. To determine the likely redshift of the blazars, we use multi-object spectroscopy to search for possible cosmic neighbours by assessing the redshifts of the galaxies in the field of view and comparing them with the previous redshift limits from direct spectroscopy and deep imaging of the blazars. A similar method has been applied to other blazars previously: PKS 0447-439 ($z = 0.343$; Muriel et al. 2015), PKS 1424+240 ($z = 0.601$; Rovero et al. 2016), PKS 2155-304 ($z = 0.116$; Farina et al. 2016), 3C 66A ($z = 0.34$; Torres-Zafra et al. 2018), PG 1553+113 ($z = 0.433$; Johnson et al. 2019), RGB 2243+203 ($z = 0.528$; Rosa González et al. 2019), and S5 0716+714 ($z = 0.23$; Pichel et al. 2023).

KUV 00311-1938 was suggested to be one of the farthest BL Lacs detected at VHE, based on a tentative redshift of $z = 0.61$ by Piranomonte et al. (2007). However, neither Pita et al. (2014) nor Pichel et al. (2021) could confirm this redshift. Pita et al. (2014) clearly identified a Mg II doublet corresponding to a redshift of $z = 0.506$, providing a lower limit for the distance of KUV 00311-1938. Pichel et al. (2021) also presented observations of 41 galaxies around this BL Lac, but due to the absence of a numerous group of galaxies, they could not conclusively determine the redshift.

For S2 0109+22, Paiano et al. (2016) derived a redshift of $z > 0.35$ through optical spectroscopy. However, they also reported the presence of a group of faint galaxies at $z \sim 0.26$, adopting photometric redshifts from the Sloan Digital Sky Survey (SDSS). The detection of the faint host galaxy in the near-IR band, as reported in MAGIC Collaboration et al. (2018), resulted in a redshift estimation of $z = 0.36 \pm 0.07$.

In this paper, we identified cosmic neighbouring galaxies around these two blazars, using both spectroscopic observations obtained from the European Southern Observatory's Very Large Telescope (VLT), in conjunction with previous observations from the literature (see Section 2), and photometric redshifts of the nearby galaxies derived from SDSS Data Release 17 (SDSS/DR17; see Section 3). Associating these cosmic neighbours with the blazars, combined with redshift constraints from previous observations, enabled us to determine a redshift of $z = 0.49$ for S2 0109+22 and a tentative redshift of $z = 0.64$ for KUV 00311-1938. We use a flat cosmology with $H_0 = 69.6$ km s^{-1} Mpc^{-1} for our calculations.

2 SPECTROSCOPIC OBSERVATIONS AND ANALYSIS

We conducted observations of the galaxies located close to KUV 00311-1938 and S2 0109+22 using the VLT's FOcal Reducer/low dispersion Spectrograph 2 (FORS2) instrument in the Multi-Object Spectrometer (MOS) mode. Additionally, we analyzed archival data from the International Gemini Observatory for both fields, acquired with the Gemini Multi Object Spectrograph (GMOS) instrument. In the following sections, we describe the data reduction processes and present the full galaxy sample, including spectroscopic and photometric redshift estimates for additional galaxies in the FORS2 fields of view, as obtained from the literature and SDSS/DR17.

2.1 FORS2

We conducted observations of 24 targets in the vicinity of KUV 00311-1938 and 30 targets in the vicinity of S2 0109+22 using FORS2/MOS on 22–23 October 2017 (P100). The selection of targets was based on their brightness and extended structure, considering the constraints imposed by the slit arrangement and available

observing time. As a result, primarily the brightest targets in the field were chosen. The ESO grism 600RI was employed, providing a wavelength range of 512–845 nm for the resulting spectra. The FORS2 chips were exposed for 600 seconds each, and this process was repeated three times. The airmass ranged from 1.1 to 1.2 for the field of KUV 00311-1938 and 1.5 to 1.6 for S2 0109+22. On October 22, 2017, the seeing ranged from 0.8 arcsec to 1.4 arcsec during the observing blocks, whereas on October 23, 2017, it varied between 0.7 arcsec and 0.9 arcsec. We processed the FORS2/MOS data using FORS pipeline release 5.5.6 in EsoRex (Freudling et al. 2013). In both fields, we utilized the same spectroscopic standard; HILT 600. We successfully processed the spectra from 21 and 15 galaxies in the field of KUV 00311-1938 and S2 0109+22, respectively. The remainder were either too faint or identified as stars.

2.2 GMOS

We retrieved the International Gemini Observatory data (observing programs GS-2016B-Q-55 and GN-2017B-Q-50; PI Pichel) from the Gemini Observatory Archive[3]. These data were acquired using GMOS on October 5, 2016, in the field-of-view of approximately 5×5 arcmin^2 centered on the blazar KUV 00311-1938. Additional data were obtained on September 27, 2017, for the field of the blazar S2 0109+22. The KUV 00311-1938 field data were obtained using the Gemini South telescope, while S20109+22 field data were acquired using the Gemini North telescope. In both cases, the exposure time for the field was 5×900s, divided for different dispersion angles (ranging from 590 nm to 630 nm), and the grating used was B600+G5323, providing a wavelength range of approximately 400–700 nm for the resulting spectra. For the KUV 00311-1938 field, the airmass ranged from 1.0 to 1.1, and seeing from 0.7 arcsec to 1.3 arcsec, with the spectroscopic standard employed being LTT 7379. In contrast, for the S2 0109+22 field, the airmass varied between 1.0 and 1.1, with seeing approximately ~0.9 arcsec, and the spectroscopic standard used was G191B2B. We processed the Gemini data using PypeIt (Prochaska et al. 2020a,b; Prochaska et al. 2020c). Out of 43 and 39 targets for the fields of KUV 00311-1938 and S2 0109+22, respectively, we successfully obtained new spectra from 11 and 23 galaxies, with the remaining targets being either too faint, acquisition targets, stars, identical to those in the FORS2 data, or located outside the FORS2 fields of view.

2.3 The full galaxy sample

For all sources, we averaged spectra from different exposures. In cases with a low signal, we also binned them by a factor of up to four. We estimated source redshifts by scaling a galaxy template spectrum, selected from five galaxy templates[4] ranging from early- to late-type, to the normalization of a given observed spectrum and shifting the wavelength to align with it.

Additionally, we complemented our sample with redshift estimates of the galaxies in the field of KUV 00311-1938 from Pichel et al. (2021), who used data from Gran Telescopio Canarias (GTC) and the MOS instrument Optical System for Imaging and low-Intermediate-Resolution Integrated Spectroscopy (OSIRIS). In total, we obtained redshift information for 39 and 38 galaxies in the fields of KUV 00311-1938 and S2 0109+22, respectively.

---

[3] https://archive.gemini.edu
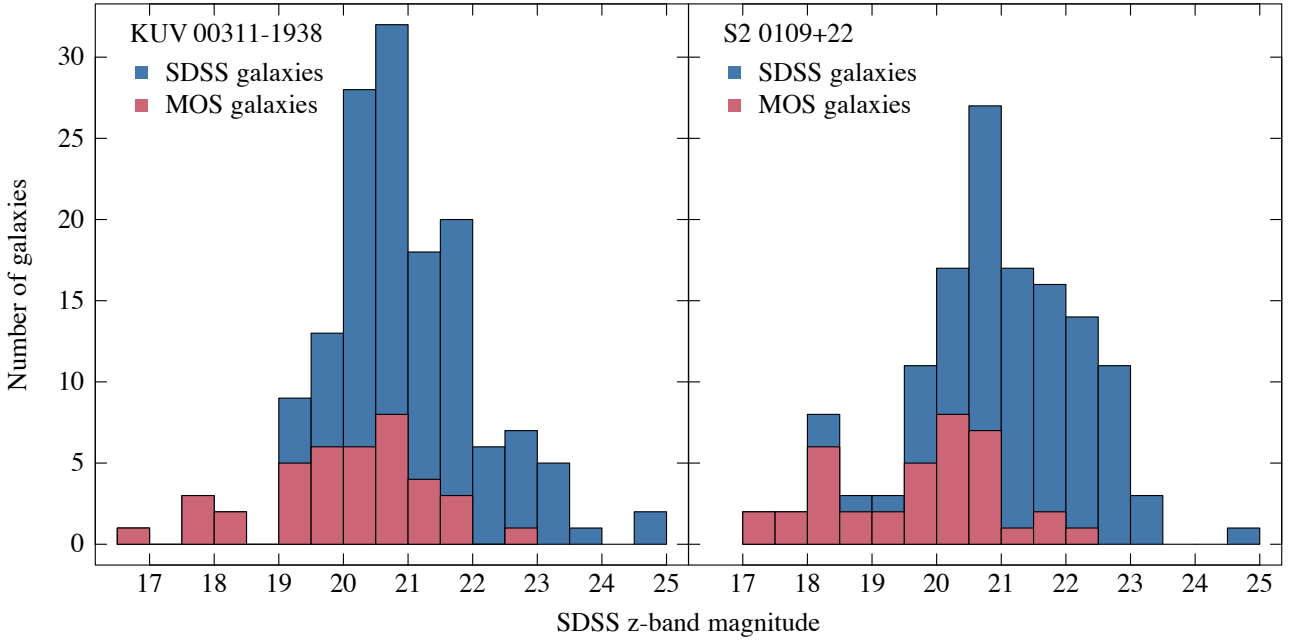[4] Obtained from https://classic.sdss.org/dr5/algorithms/spectemplates

Figure 1. SDSS z-band magnitude histograms of the sources located in the fields of view of the FORS2 observations shown in Figs. 2 and 4. Sources probed by the MOS observations studied in this paper are highlighted in red, while all identified SDSS galaxies are highlighted in blue.

We also obtained photometric redshifts for all galaxies in both fields from SDSS/DR17 (Abdurro'uf et al. 2022) and compared them to spectroscopic redshifts obtained in our work and previous studies. We noticed that a few redshifts derived in earlier studies deviated significantly ($> 3\sigma$) from the photometric redshift estimates. Comparing our derived redshifts from Gemini data to those reported by Pichel et al. (2020, 2021), we observed agreement for all galaxies except for seven (slits 7, 19, 20, 24, 27, and 29 for the field of S2 0109+22, and slit 29 for the field of KUV 00311-1938). In this paper, we use the results of our new analysis throughout.

Fig. 1 displays the SDSS z-band magnitude histograms of both fields, with the VLT, Gemini, and GTC targets highlighted in red, alongside all identified galaxies in the SDSS/DR17 shown in blue. It is evident that our targets do not constitute a complete flux or volume limited sample.

3 RESULTS AND DISCUSSION

The estimated spectroscopic redshifts of all galaxies used in this work are presented in Figs. 2–5, displayed as mosaic images and histograms to identify potential groups of galaxies sharing similar redshifts. It is important to note that these identified groups of cosmic neighbors may not necessarily be genuine galaxy groups; they could also include galaxies from neighboring groups or be part of the same cluster of galaxies. This ambiguity arises because, in this redshift range, we only observe the brightest galaxies in the groups. For simplicity, however, we refer to them as 'group candidates' in the following sections. Detailed redshift data for the galaxies can be found in Tables A1 and A2.

By combining our FORS2 data with reanalyzed Gemini data and incorporating GTC galaxies from Pichel et al. (2021), we have identified multiple galaxy group candidates in the field of KUV 00311-1938. Specifically, there are two group candidates with four members each, located at $z = 0.147 - 0.148$, and $z = 0.237 - 0.240$, respectively. Additionally, there is one group candidate with five

members at $z = 0.411 - 0.414$. Furthermore, two galaxy pairs are found at $z = 0.533 - 0.535$, and $z = 0.639 - 0.640$. Similarly, in the field of S2 0109+22, we have identified two group candidates, each with seven members, located at $z = 0.1835 - 0.1867$ and $z = 0.2662 - 0.2694$, respectively. Additionally, there is one group candidate with five members at $z = 0.490 - 0.495$.

3.1 Comparison with previous redshift limits

Previous redshift limits for both sources were determined through direct optical spectroscopy and Very High Energy (VHE) γ-ray observations. Lower limits from optical spectroscopy are derived either by detecting lines from intervening absorption systems (Pita et al. 2014) or, in cases where no lines are detected, by assuming that the host galaxy of the blazar is a giant elliptical galaxy and estimating how faint the galaxy must be for its lines not to be detected in the obtained spectrum (Sbarufatti et al. 2006; Paiano et al. 2016). On the other hand, upper limits for redshifts from the γ-ray spectrum, based on EBL absorption arguments, have also been established for both sources. Abdalla et al. (2020) set an upper limit of $z < 0.98$ for KUV 00311-1938, while MAGIC Collaboration et al. (2018) reported an upper limit of $z \leq 0.67$ for S2 0109+22. These upper limits exceed the redshifts of the group candidates we detected in the fields of these two blazars, thus confirming all identified group candidates as potential associations with the blazar. However, in the following, we will compare the spectroscopic lower limits with the redshifts of the group candidates identified in our analyses.

In the case of KUV 00311-1938, Pita et al. (2014) obtained an X-Shooter spectrum, and the UVB arm spectrum revealed a Mg II doublet at 4215Å, corresponding to a redshift of $z = 0.506$. This serves as a strict lower limit to the blazar's redshift. This finding makes the association with the most numerous group candidates at $z = 0.147 - 0.148$, $z = 0.237 - 0.240$, and $z = 0.411 - 0.414$ unfeasible. No companion galaxies were detected at the distance of $z \sim 0.5$. If the absorption system is intrinsic to the host galaxy, this
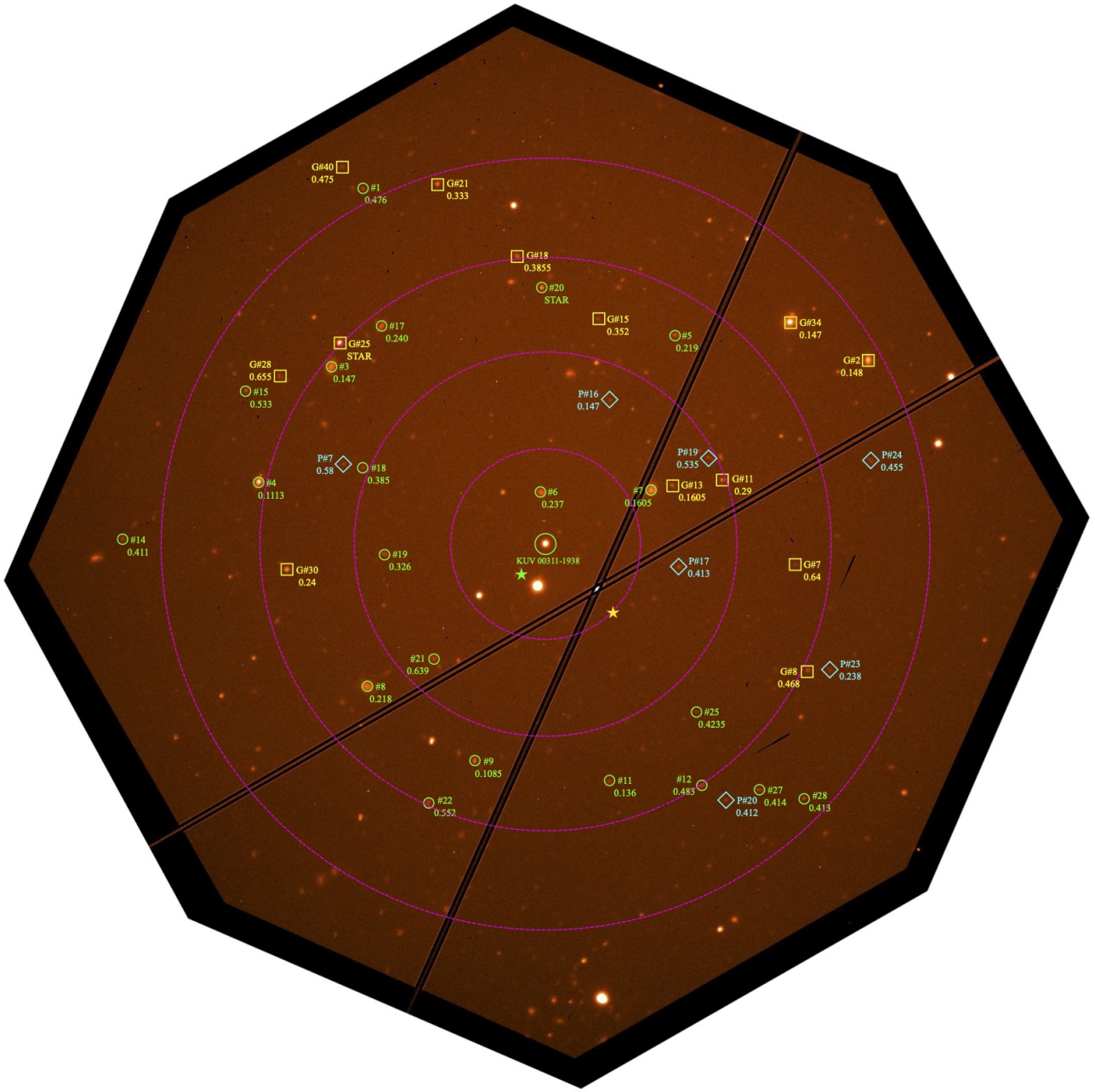
Figure 2. Mosaic R-band image of the field of KUV 00311-1938 taken with FORS2 from our observations. The green circles indicate the sources observed with FORS2 MOS, the yellow squares indicate the sources observed with Gemini, and the blue diamonds mark the GTC sources from Pichel et al. (2021). Corresponding source redshifts are shown along with the source numbering. Sources with a stellar spectrum are marked as 'STAR'. Magenta dashed lines show angular radii of 0.5, 1.0, 1.5, and 2.0 Mpc at a redshift of $z = 0.64$ (the most likely distance of the blazar based on our analysis). The yellow and green stars show the center locations of the spectroscopic and photometric groups at $z = 0.64$ and $z = 0.7$, respectively, derived from our analysis. The black lines crossing the image come from chip gaps and the image is cropped to show only the area covered by the two exposures.

suggests that KUV 00311-1938 is isolated at this distance. However, since our sample does not encompass all galaxies in the field, we might have missed the ones at this particular distance. In addition, there could be an intervening cold system absorbing the blazar light along the line-of-sight at $z = 0.506$, but the blazar itself could be positioned farther away. We identified two galaxy pairs situated at $z = 0.533 - 0.535$ and $z = 0.639 - 0.640$, which could potentially be cosmic neighbours of the blazar. We will further evaluate this possibility in the following sections.

For S2 0109+22, Paiano et al. (2016) presented a GTC spectrum

of the blazar, which did not reveal discernible line features. They simulated source spectra by assuming an absolute magnitude for the host galaxy of $M_{R, Vega}$ = -22.9 mag. If the blazar were associated with the group candidate at $z = 0.265$, Ca II and G-band lines would have been visible in the GTC spectrum. Consequently, they suggested a redshift of $z > 0.35$ based on the assumed brightness of the host galaxy.

We repeated this simulation analysis at three different redshifts: $z = 0.18$, $z = 0.26$, and $z = 0.49$, as determined by our spectroscopic galaxy group candidate analysis. In each case, the apparent R-band
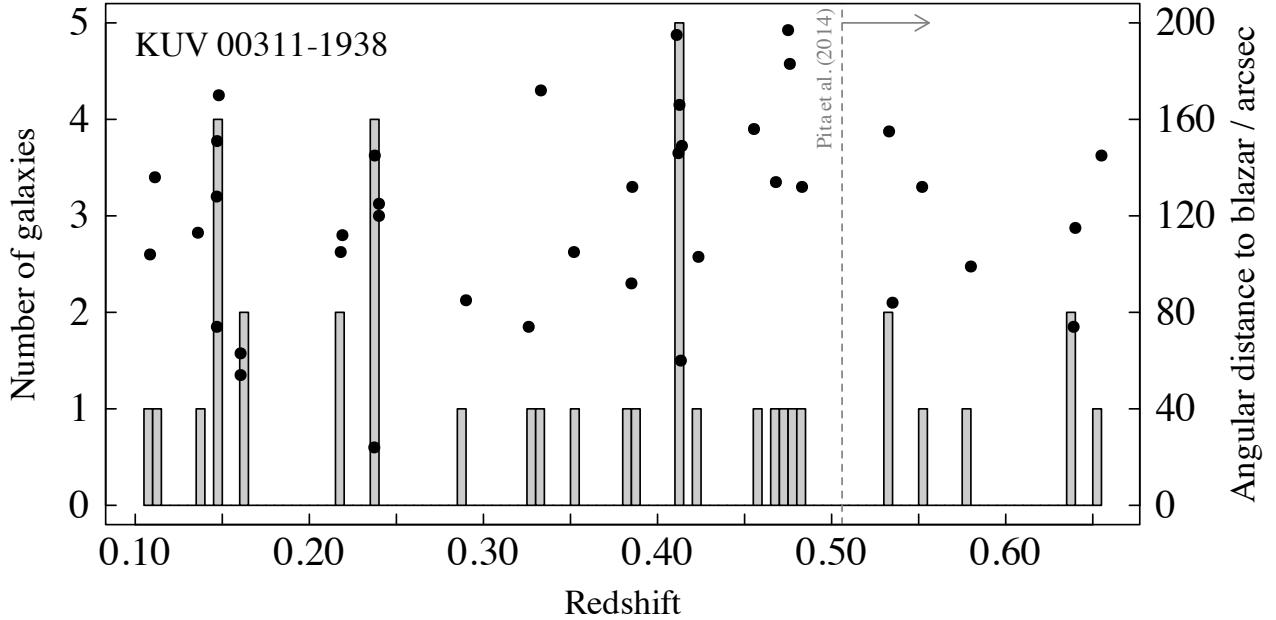
Figure 3. Redshift histogram of all galaxies studied in this paper in the field of KUV 00311-1938 (see Fig. 2). The individual galaxy redshifts are also plotted as points, indicating their angular distance from the blazar position. The field contains two galaxy groups with four members each and one with five. A distance lower limit from the literature is shown as a dashed line.

magnitude of S2 0109+22 was assumed to be $m_{R,Vega}$ = 14.8 mag, as reported in Paiano et al. (2016). Consequently, the core-to-host flux ratio increased from 5.9 to 80 as the redshift increased from $z = 0.18$ to $z = 0.49$. We assumed a magnitude of $M_{R,Vega}$ = -22.9 mag and an effective radius of 9 kpc for the host galaxy, applied the K- and evolution corrections, and accounted for the slit losses, which varied with redshift for both the core and the host galaxy. While Paiano et al. (2016) did not specify the full width at half maximum (FWHM) of their observation, assuming FWHM = 0.7 arcsec provided a very accurate reproduction of the correct flux level. Finally, we introduced Gaussian noise with the same characteristics as in the observed spectrum into the simulation.

Figure 6 illustrates the results of the simulations. A visual inspection of the spectra clearly indicates that the host galaxy absorption lines would certainly be detectable at $z = 0.18$ and very likely at $z = 0.26$. In contrast, at $z = 0.49$, they would be impossible to detect. This supports the conclusion by Paiano et al. (2016) that the redshift is likely to be larger than $z > 0.35$, suggesting that the most numerous candidate groups in the field are likely to be foreground groups.

We previously conducted deep imaging of S2 0109+22 and detected the host galaxy with an apparent I-band magnitude of $m_{I,Vega}$ = 18.05 mag (MAGIC Collaboration et al. 2018). In that study, assuming the host galaxy to be a giant elliptical galaxy with $M_{R,Vega}$ = -22.8±0.5 mag, we utilized the method of Sbarufatti et al. (2005) to derive an imaging redshift of $z = 0.36 \pm 0.07$. The association with a more distant candidate group suggests that the host galaxy is somewhat more luminous, $M_{R,Vega}$ = -23.8±0.5 mag, than typical blazar host galaxies. This aligns with our findings in Nilsson et al. (2003): while imaging redshifts agree very well at redshifts $z < 0.3$, at higher redshifts, we tend to detect only the most luminous host galaxies, making the imaging redshifts less accurate.

Table 1. Chance coincidence probabilities for several parameter sets using the galaxy group catalogue from zCOSMOS.

Redshift	N	prob	prob×0.3
KUV-like params:			
$0.50 < z < 0.65$	≥ 2	0.56	0.17
	≥ 3	0.22	0.066
S2-like params:			
$0.49 < z < 0.85$	≥ 5	0.18	0.054
	≥ 6	0.12	0.036

3.2 The probability of observing galaxy groups by chance

To assess the probability that the observed galaxy group candidates occur in the fields by chance, we followed the methodology outlined in Rovero et al. (2016). We utilized the galaxy group catalogue, zCOSMOS[5], containing groups within the redshift range of $0.1 < z < 1.0$, and an apparent magnitude range of $m_{I,AB} < 22.5$ mag, to randomly select positions in the sky. This process was based on the assumption that the sky exhibits similar characteristics throughout, as the zCOSMOS field is relatively small and not positioned in the same location as the source. In addition, since our sample is not complete to $m_{I,AB} \approx m_{z,AB} < 22.5$ mag, this estimation is conservative, as we are very likely missing members from our candidate groups. This enabled us to determine the likelihood of a coincidental presence of groups with a specified minimum number in the observed field. The resulting coincidence probabilities are detailed in Table 1 for both fields, various redshift ranges, and sizes of galaxy groups.

Furthermore, assessing the distance between galaxies within galaxy groups and the blazar can help estimate the likelihood of association. Galaxy groups typically have sizes smaller than 2 Mpc

---

[5] https://github.com/wkcosmology/zCOSMOS-bright_group_catalog
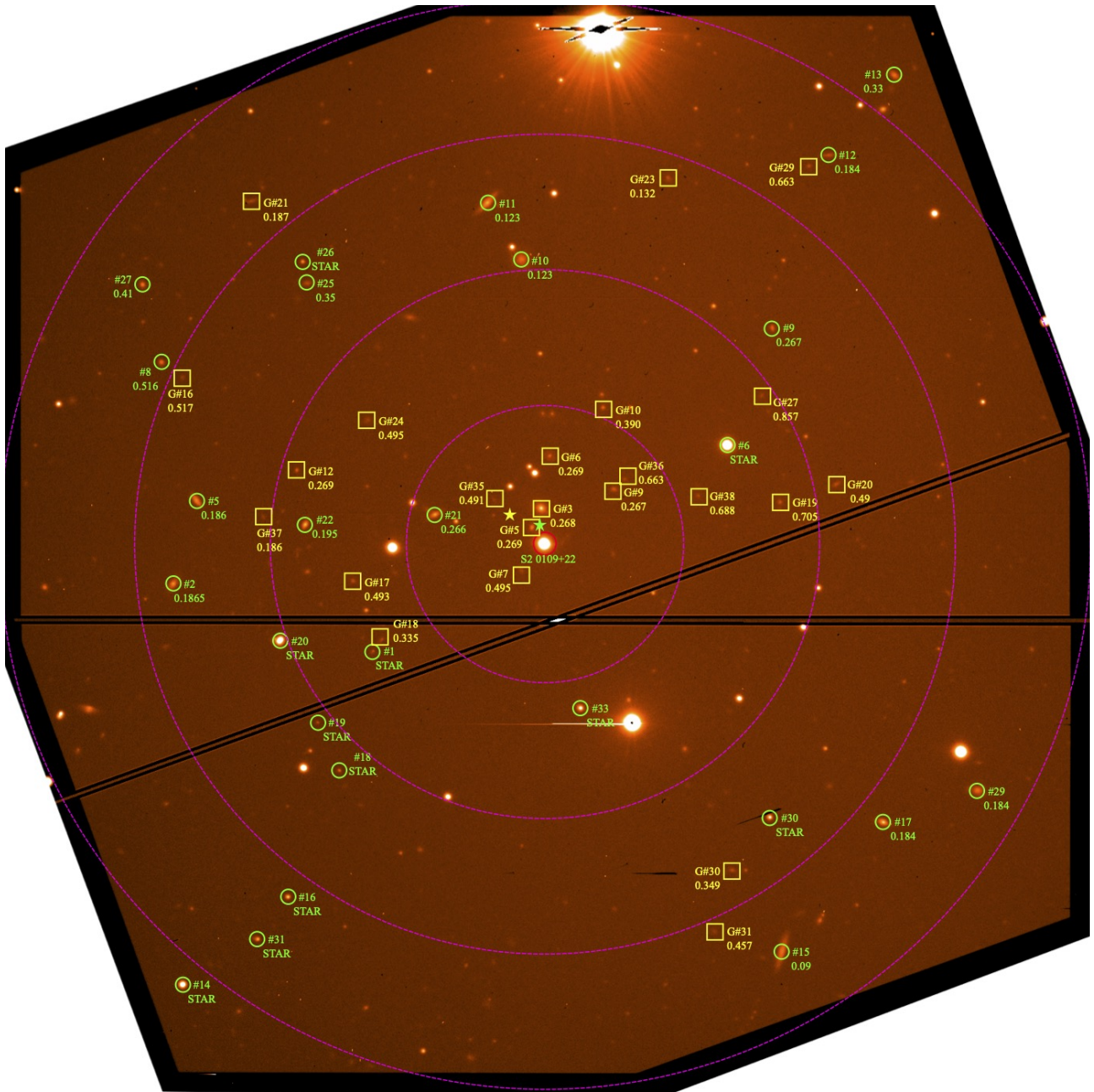
Figure 4. Mosaic R-band image for S2 0109+22 taken with FORS2 from our observations. The green circles indicate the sources observed with FORS2 MOS, and the yellow squares indicate the sources observed with Gemini. Corresponding source redshifts are shown along with the source numbering. Sources with a stellar spectrum are marked as 'STAR'. Magenta dashed lines show angular radii of 0.5, 1.0, 1.5, and 2.0 Mpc at a redshift of $z = 0.49$ (the most likely distance of the blazar based on our analysis). The yellow and green stars show the center locations of the spectroscopic and photometric groups at $z = 0.49$, respectively, derived from our analysis. The black lines crossing the image come from chip gaps and the image is cropped to show only the area covered by the two exposures.

(see e.g. Tago et al. 2010), making this a common search radius for cosmologically neighboring galaxies. Massaro et al. (2019, 2020a,b) investigated groups around radio galaxies and BL Lac objects, revealing that if there are two companions at the same redshift ($z < 0.005$) within a distance of 1.0 Mpc from the blazar and/or four companions within 2.0 Mpc, the probability of the blazar being associated with that group exceeds 95%. In addition to distance, the location within the group is important. Massaro et al. (2019, 2020a,b) noted that blazars tend to be positioned at the group centers. Utilizing Galaxy and Mass assembly data at higher redshifts ($0.1 < z < 0.35$), Wethers et al. (2022) observed a similar tendency for quasars in gen-

eral. Although these studies do not cover the redshift range of our candidate groups and may not be directly applicable to our objects, we nonetheless explored the virial radii of the candidate groups and the position of the blazar within each candidate group.

For KUV 00311-1938, the estimated virial radii of the candidate group, which includes the blazar and the pair of galaxies at $z = 0.533 - 0.535$ or $z = 0.639 - 0.640$, are 1.25 Mpc and 1.21 Mpc, respectively. These values are notably larger than typical galaxy group sizes (see e.g. Nurmi et al. 2013). Therefore, instead of constituting galaxy groups, they are likely neighbouring groups, and we observe only the brightest galaxies from these structures. Addition-
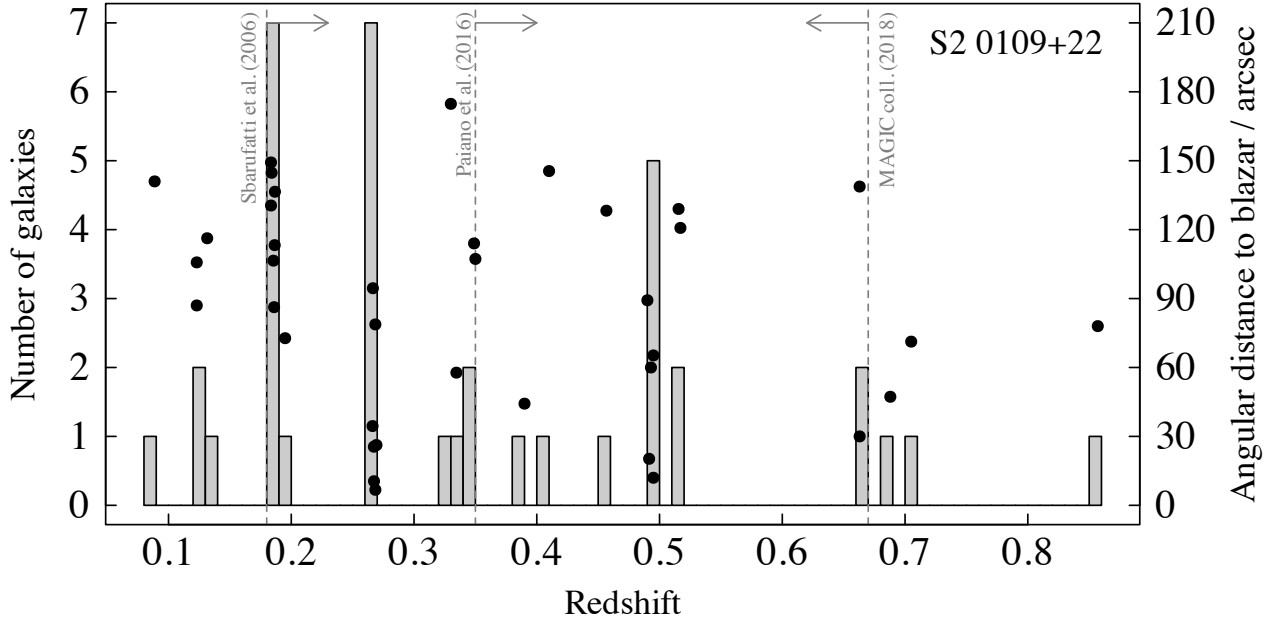
Figure 5. Redshift histogram of all galaxies studied in this paper in the field of S2 0109+22 (see Fig. 4). The individual galaxy redshifts are also plotted as points, indicating their angular distance from the blazar position. The field contains three galaxy groups with either five or seven members. Three distance lower/upper limits from the literature are shown as dashed lines.
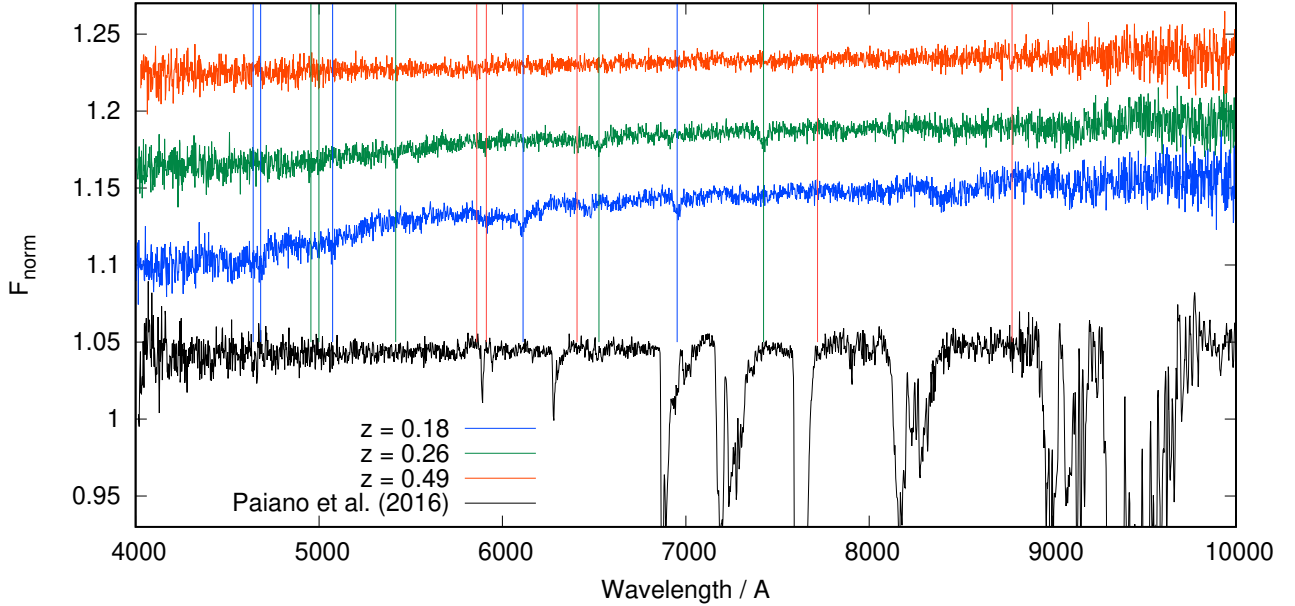

Figure 6. Simulated spectra of S2 0109+22 at the three redshifts discussed in the text and the spectrum from Paiano et al. (2016). We assumed a magnitude of $M_{R, Vega} = -22.9$ mag for the host galaxy. All spectra have been normalized by a power-law continuum with a slope -0.56. The spectra have been shifted vertically for clarity. The vertical lines indicate the positions of the (from left to right) Ca K, Ca H, G-band, Mg b, and Na D lines with the same color coding as the spectra.

ally, we computed the geometrical center for the pairs, and in both cases, they are within a few hundred kiloparsecs from the blazar. The central point for the group at $z = 0.639 - 0.640$ is marked by a green star in Fig. 2.

In the case of S2 0109+22, there are five galaxies in the candidate group at $z = 0.49$ that may be associated with the blazar. Assuming the blazar belongs to this group, we derive a virial radius of 0.35 Mpc,

falling within the range derived for luminous groups in Nurmi et al. (2013). Additionally, the geometrical center of this candidate group is very close to the blazar (see Fig. 4).

3.3 Search for possible groups using photometric redshifts

We obtained the photometric redshifts for galaxies within our fields of view using SDSS/DR17, resulting in 52 and 36 redshift estimates for the fields of KUV 00311-1938 and S2 0109+22, respectively. To assess potential galaxy group candidates based on the photometric redshift data, we created kernel density estimates (KDEs) of the redshift distributions, assuming a Gaussian distribution with a centroid and width corresponding to the values tabulated in SDSS/DR17. The corresponding KDEs, including a combined one, are depicted in Fig. 7 and Fig. 8 for both fields.

Assuming that the combined KDE is primarily composed of a few galaxy groups (neglecting lower-level 'noise' from individual galaxies situated at random distances), we can approximate the combined KDEs using a few Gaussian components (colored dashed lines in Figs. 7 and 8) representing the individual groups. These Gaussian components have centroids at the group redshift and widths similar to the mean error of the photometric redshift values in SDSS/DR17 ($\Delta z \sim 0.12$). We note again that, for simplicity, we refer to these groupings as 'group candidates', but they are more likely to trace some larger structure such as neighbouring groups or a cluster.

For KUV 00311-1938, we fitted the combined KDE with three Gaussian components. These three Gaussians, representing three galaxy group candidates, adequately account for the overall galaxy distribution. The Gaussian centroids of the two lower redshift groups closely align with the redshifts of the group candidates obtained from the multi-object spectroscopy, considering that the group candidates at $z = 0.18$ and $z = 0.27$ are likely blended with each other. Additionally, a third group candidate at $z \sim 0.68$ is necessary to explain the combined KDE at higher redshifts. This peak is sufficiently prominent in the field, suggesting it may represent a potential galaxy group located approximately at that distance, which could be associated with the blazar. In the spectral analysis, we identified a galaxy pair at a redshift of $z = 0.639 − 0.640$ that could represent galaxies in this group candidate, favoring this redshift over the other galaxy pair at z= $0.533 − 0.535$. Nevertheless, this remains a tentative association, and further data would be required to confirm it.

Similar to KUV 00311-1938, the galaxy distribution in the field of S2 0109+22 can be represented by three Gaussian components. Their centroid values again closely match those obtained through our spectroscopic analysis. However, the third group candidate identified in our spectral analysis at $z = 0.19$ is not clearly discernible in the combined KDE, likely because the redshift is quite close to the group at $z = 0.27$. Thus, the SDSS photometric redshifts of galaxies in the field of S2 0109+22 support the existence of the three group candidates identified in our spectral analysis.

Finally, we calculated the 'composite' group central location by weighting the coordinates (RA/Dec) of each galaxy according to the Gaussian distribution of a given group and based on the individual galaxy redshifts (i.e., the weight would be unity if the redshift of a galaxy matches the peak redshift of the Gaussian component and gradually diminishes towards the tails of the distribution). As mentioned above, it is reasonable to assume that blazars should be situated near the center of their associated group candidates (Massaro et al. 2019, 2020a). Therefore, the closer the group candidate center is to the blazar, the more likely the association. We computed the geometrical center of the candidate groups in both fields, and their separation from the blazar is marked in Figs. 7 and 8. In the field of KUV 00311-1938, the weighted group centers are roughly equally proximate to the blazar. However, in the field of S2 0109+22, the weighted group center close to the redshift of $z = 0.49$ (group I

in Fig. 8) is notably much closer than the other two, further strengthening its association with the blazar.

3.4 The probability that a blazar is not associated with any group

It is possible that the blazar is isolated and not associated with any group that may be present in the field. However, there are limited studies to accurately quantify this. Muriel (2016) analyzed a sample of approximately 120 blazars and determined that 32±4% of them exist as single sources, while 43±5% are found in groups containing three or more members. Nevertheless, Massaro et al. (2020a) critiqued the sample used in this study, concluding that only 14 sources of the sample were genuinely blazars. Among these 14, four were discovered to be isolated (i.e., 29%), and seven were found in groups of three or more members (i.e., 50%), aligning with Muriel (2016). It is worth noting that the blazars examined in these studies have redshifts less than $z < 0.2$. Based on the above, it appears that approximately 30% of blazars tend to be isolated. This probability is independent of the likelihood of finding groups in a random position in the sky. Consequently, the combined probabilities of having a non-associated galaxy group in the same field with the blazar are tabulated in Table 1. Essentially, the probability that the blazar S2 0109+22 is isolated and the field coincidentally hosts a galaxy group of five or more members above the redshift of $z > 0.49$ is quite low, at about 5%. In the case of KUV 00311-1938, the probability is somewhat higher, approximately 15%, primarily due to the smaller size of the 'groups' above $z > 0.5$. Nonetheless, it is important to consider these as conservative estimates. As shown in Fig. 1, our galaxy sample is not complete in the field, particularly at higher redshifts, which makes it likely that we are missing members from the group candidates.

3.5 Prospects for using KUV 00311-1938 and S2 0109+22 to detect warm-hot intergalactic medium

A significant portion of the baryons predicted by the current leading cosmological theory (λCDM) remains undetected (e.g. Shull et al. 2012; Danforth et al. 2016). Cosmological simulations indicate that these missing baryons reside in the WHIM phase embedded in the filaments of the Cosmic Web (e.g. Cen & Ostriker 1999; Martizzi et al. 2019). However, due to its low density, the expected X-ray emission from the WHIM is at or beyond the capabilities of current instrumentation. Instead, the WHIM could be detected as an absorption feature in the X-ray spectra of bright blazars located behind the WHIM filaments (see e.g. Fang et al. 2007; Bonamente et al. 2016; Ahoranta et al. 2020, for possible detections).

WHIM filaments can be traced by galaxy groups in SDSS up to $z = 0.155$, but the sample is only homogeneous up to $z = 0.05 − 0.06$ (Tempel et al. 2014). Therefore, although our observations indicate the presence of foreground groups or structures at $z = 0.15 − 0.26$ for both blazars, it is impossible to ascertain if these groups trace filamentary structures with sufficient WHIM column density. Significant improvement in this regard is expected with the 4MOST 4HS survey, where the chances of intercepting an absorbing system are anticipated to increase to a level of ~50% per sight line (Tuominen et al. 2023).

Both blazars are X-ray bright with fluxes of F(0.3–10 keV)= 7.2×10^{-12} erg/cm^2/s (KUV 00311-1938, Tavecchio et al. 2010) and F(0.3–10 keV)= $(2.5 − 15) \times 10^{-12}$ erg/cm^2/s (S2 0109+22, MAGIC Collaboration et al. 2018). These fluxes are sufficiently high to observe X-ray absorption features, similar to, for example, H 2356-309,
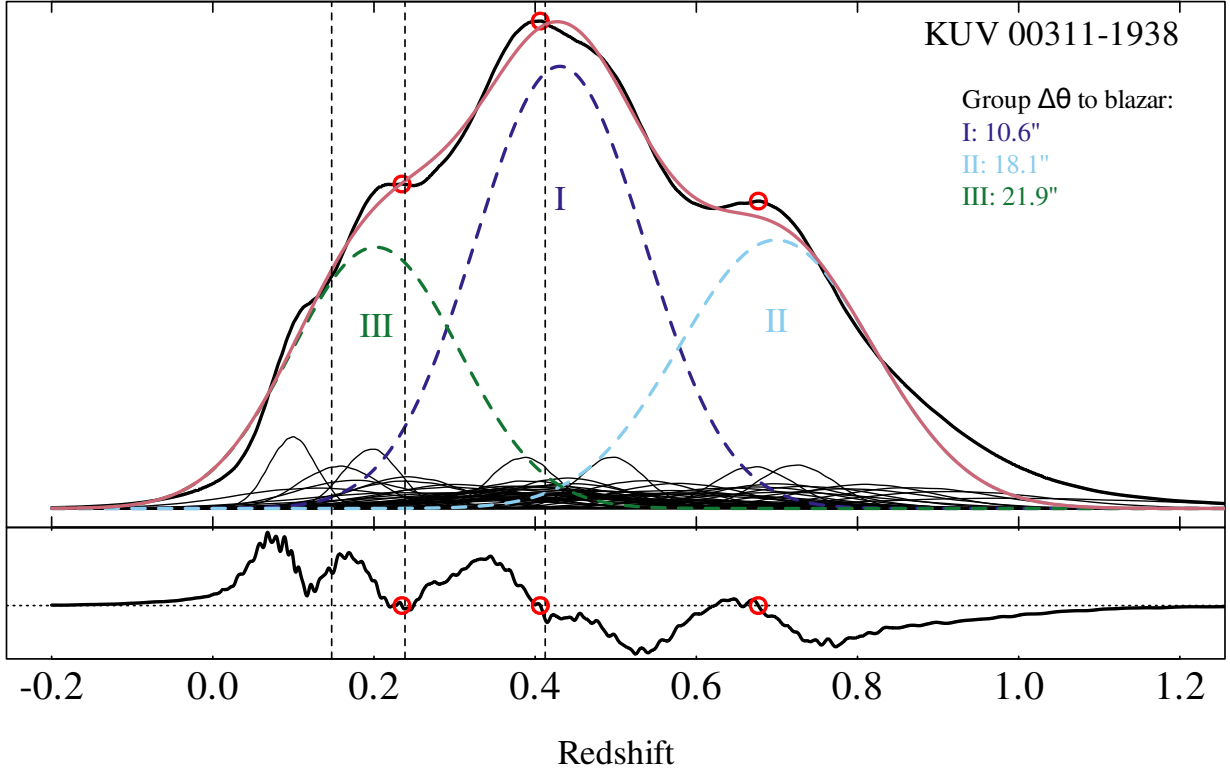
Figure 7. A KDE analysis for the SDSS/DR17 photometric redshift distributions of galaxies within 2' from KUV 00311-1938. *Upper panel:* The solid thin black lines show the KDEs for single galaxies in the field; the thick solid black line is their sum. The solid red line shows the estimated galaxy distribution in the field assuming that it consists mostly of a few individual galaxy groups (in this case three; colored dashed lines and marked with roman numerals). The average, weighted group center separation to the location of the blazar is marked in the figure legend. *Lower panel:* Local derivative of the summed KDE. Red circles show the crossing points of the derivative from positive to negative values marking the locations of local maxima in the summed KDE (shown also in the upper panel). Black vertical dashed lines show the locations of the galaxy groups in the field from our spectral analysis. They match well with the zero crossings and peaks of the individual Gaussian profiles (I and III). The KDE analysis suggests an additional galaxy group in the field at z~0.68 (II) not picked up by the spectral analysis that could be associated with the blazar.

which has been utilized in such studies by Zappacosta et al. (2010). Consequently, both blazars could be intriguing sources for investigating WHIM at higher redshifts with new or upcoming X-ray missions such as XRISM and NewAthena.

4 CONCLUSIONS

In this paper, we identified several galaxy group candidates in the fields of both blazars, KUV 00311-1938 and S2 0109+22, through both our spectroscopic observations and our analysis of the distribution of photometric redshifts. We utilized previous direct optical spectroscopy limits to discern which of these groups are likely foreground groups. In both cases, we also observed galaxies with higher redshifts that could potentially be associated with the blazar.

Even before our study, KUV 00311-1938 was known to be within a redshift range where only a handful of VHE γ-ray emitting objects are available for indirect EBL studies. We did not detect any galaxies at redshift $z = 0.506$, which is the lower limit from direct spectroscopy based on the Mg II absorption line. Most of the galaxies we observed in spectroscopy turned out to be members of foreground groups. Intriguingly, our KDE analysis of the photometric redshifts suggests the presence of an additional galaxy group at $z \sim 0.68$. Two of the galaxies we observed have spectroscopic redshifts $z = 0.639 - 0.640$, but since they are only two, the probability

of a chance coincidence is high (~15%). A spectroscopic follow-up of the galaxies with photometric redshifts of $z \sim 0.68$ could confirm this high redshift.

For S2 0109+22, we found a group of five galaxies with a redshift of $z = 0.49$, and the chance probability for this association is low (~5%). This association is further supported by our KDE analysis results, where we also identified this group. Both in spectroscopic and photometric analysis, the weighted central points of the candidate group lie very close to the blazar. Therefore, we conclude that the blazar very likely belongs to this candidate group and has a redshift of $z = 0.49$.

In summary, we have demonstrated in this work that combining spectroscopic redshifts with an analysis of the photometric redshifts of galaxies around the blazar with an unknown redshift allowed us to determine the likely redshifts for both blazars. In the case of KUV 00311-1938, further confirmation of this high redshift could be achieved with additional observations. Many of the galaxies we used in this work have r-band magnitudes larger than 20, and therefore, spectroscopy still requires dedicated observations with rather large telescopes. Nevertheless, with upcoming surveys such as 4MOST coming online in the next few years, this method of determining the redshifts will become feasible for a larger sample of blazars. This will also help indentify the most suitable blazars for studies of extragalactic background light and the warm-hot intergalactic medium.
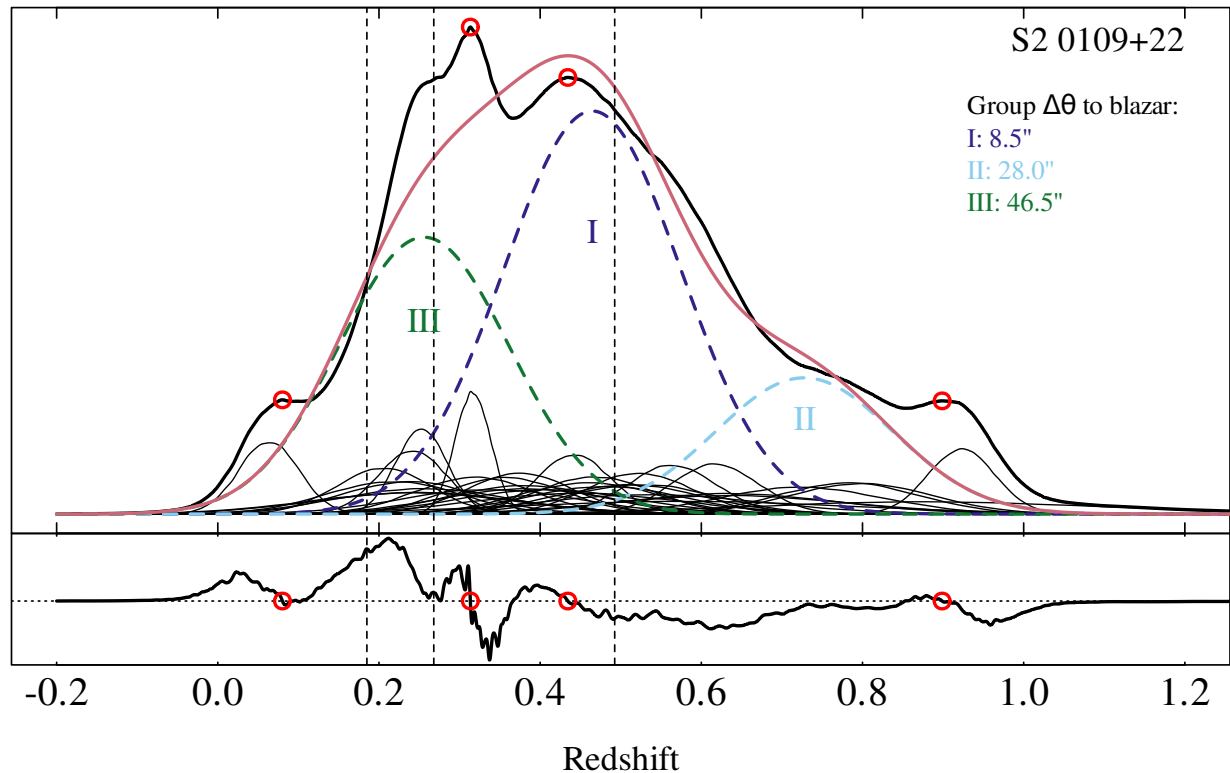
Figure 8. A KDE analysis for the SDSS/DR17 photometric redshift distributions of galaxies within 2' from S2 0109+22 similar to Figure 7. The peaks of the individual Gaussian profiles (I and III) match well with the spectrometric redshifts, while the local maxima are dominated by KDEs from single sources. The average weighed group centers suggest group I as the most probable association to the blazar.

DATA AVAILABILITY

The VLT/FORS2 data analyzed here are available at the European Southern Observatory Science Archive Facility (`http://archive.eso.org`). The Gemini data is available at the Gemini Observatory archive (`https://archive.gemini.edu`). The SDSS data is available at the SDSS website: `https://www.sdss4.org`. The simulation data produced as part of this work are available from the authors on request.

REFERENCES

Abdalla H., et al., 2020, MNRAS, 494, 5590
Abdalla H., et al., 2021, J. Cosmology Astropart. Phys., 2021, 048
Abdurro'uf et al., 2022, ApJS, 259, 35
Acciari V. A., et al., 2019, MNRAS, 486, 4233
Ahoranta J., et al., 2020, A&A, 634, A106
Bonamente M., Nevalainen J., Tilton E., Liivamägi J., Tempel E., Heinämäki P., Fang T., 2016, MNRAS, 457, 4236
Cen R., Ostriker J. P., 1999, ApJ, 514, 1
Danforth C. W., Keeney B. A., Stocke J. T., Shull J. M., Yao Y., 2010, ApJ, 720, 976
Danforth C. W., et al., 2016, ApJ, 817, 111
Dorigo Jones J., et al., 2022, MNRAS, 509, 4330
Fang T., Canizares C. R., Yao Y., 2007, ApJ, 670, 992
Farina E. P., Fumagalli M., Decarli R., Fanidakis N., 2016, MNRAS, 455, 618
Freudling W., Romaniello M., Bramich D. M., Ballester P., Forchi V., García-Dabló C. E., Moehler S., Neeser M. J., 2013, A&A, 559, A96
Fumagalli M., Dessauges-Zavadsky M., Furniss A., Prochaska J. X., Williams D. A., Kaplan K., Hogan M., 2012, MNRAS, 424, 2276
Furniss A., et al., 2013, ApJ, 768, L31
Goldoni P., et al., 2021, A&A, 650, A106
IceCube Collaboration et al., 2018, Science, 361, 147
Johnson S. D., et al., 2019, ApJ, 884, L31
Kasai E., et al., 2023, MNRAS, 518, 2675
MAGIC Collaboration et al., 2018, MNRAS, 480, 879
Martizzi D., et al., 2019, MNRAS, 486, 3766
Massaro F., Álvarez-Crespo N., Capetti A., Baldi R. D., Pillitteri I., Campana R., Paggi A., 2019, ApJS, 240, 20
Massaro F., et al., 2020a, ApJS, 247, 71
Massaro F., Capetti A., Paggi A., Baldi R. D., Tramacere A., Pillitteri I.,

Campana R., 2020b, ApJ, 900, L34

Muriel H., 2016, A&A, 591, L4

Muriel H., Donzelli C., Rovero A. C., Pichel A., 2015, A&A, 574, A101

Nilsson K., Pursimo T., Heidt J., Takalo L. O., Sillanpää A., Brinkmann W., 2003, A&A, 400, 95

Nurmi P., et al., 2013, MNRAS, 436, 380

Paiano S., Landoni M., Falomo R., Scarpa R., Treves A., 2016, MNRAS, 458, 2836

Paiano S., Landoni M., Falomo R., Treves A., Scarpa R., 2017, ApJ, 844, 120

Paiano S., Falomo R., Treves A., Scarpa R., 2020, MNRAS, 497, 94

Paiano S., Falomo R., Treves A., Padovani P., Giommi P., Scarpa R., 2021, MNRAS, 504, 3338

Pichel A., Donzelli C., Muriel H., Rovero A. C., 2020, Boletin de la Asociacion Argentina de Astronomia La Plata Argentina, 61B, 186

Pichel A., et al., 2021, PASP, 133, 014102

Pichel A., et al., 2023, A&A, 680, A52

Piranomonte S., Perri M., Giommi P., Landt H., Padovani P., 2007, A&A, 470, 787

Pita S., et al., 2014, A&A, 565, A12

Prochaska J. X., et al., 2020a, pypeit/PypeIt: Release 1.0.0, doi:10.5281/zenodo.3743493

Prochaska J. X., Hennawi J. F., Westfall K. B., Cooke R. J., Wang F., Hsyu T., Davies F. B., Farina E. P., 2020b, arXiv e-prints, p. arXiv:2005.06505

Prochaska J. X., et al., 2020c, Journal of Open Source Software, 5, 2308

Rees M. J., Begelman M. C., Blandford R. D., Phinney E. S., 1982, Nature, 295, 17

Rosa González D., et al., 2019, MNRAS, 482, 5422

Rovero A. C., Muriel H., Donzelli C., Pichel A., 2016, A&A, 589, A92

Sbarufatti B., Treves A., Falomo R., 2005, ApJ, 635, 173

Sbarufatti B., Falomo R., Treves A., Kotilainen J., 2006, A&A, 457, 35

Shull J. M., Smith B. D., Danforth C. W., 2012, ApJ, 759, 23

Tago E., Saar E., Tempel E., Einasto J., Einasto M., Nurmi P., Heinämäki P., 2010, A&A, 514, A102

Tavecchio F., Ghisellini G., Ghirlanda G., Foschini L., Maraschi L., 2010, MNRAS, 401, 1570

Tempel E., et al., 2014, A&A, 566, A1

Torres-Zafra J., Cellone S. A., Buzzoni A., Andruchow I., Portilla J. G., 2018, MNRAS, 474, 3162

Tuominen T., Nevalainen J., Heinämäki P., Tempel E., Wijers N., Bonamente M., Aragon-Calvo M. A., Finoguenov A., 2023, A&A, 671, A103

Wethers C. F., et al., 2022, ApJ, 928, 192

Zappacosta L., Nicastro F., Maiolino R., Tagliaferri G., Buote D. A., Fang T., Humphrey P. J., Gastaldello F., 2010, ApJ, 717, 74

APPENDIX A: GALAXY DISTANCE TABLE

This paper has been typeset from a TeX/LaTeX file prepared by the author.

Table A1. Properties of the galaxies in the field of KUV 00311-1938. Columns are (1) right ascension in degrees, (2) declination is degrees, (3) SDSS z'-band magnitude, (4) redshift from multi-object spectroscopy, (5) instrument used to obtain the spectrum, (6) SDSS photometric redshift, (7) separation to blazar in arcseconds, and (8) source numbering shown in Fig. 2.

RA (deg)	DEC (deg)	z'$_{AB}$ (mag)	SpecZ	Inst.	PhotoZ SDSS	$\Delta\theta$ (")	N
8.348750	-19.34886	21.05±0.17	0.4554	OSIRIS	0.49±0.17	156	#24
8.349691	-19.33609	17.83±0.03	0.1480	GMOS	0.12±0.03	170	G#2
8.354167	-19.37567	21.94±0.12	0.2376	OSIRIS	0.25±0.12	145	P#23
8.357860	-19.37570	20.07±0.08	0.4680	GMOS	0.45±0.08	134	G#8
8.358805	-19.39175	21.38±0.13	0.4126	FORS2	0.32±0.13	166	#28
8.359580	-19.36220	20.75±0.05	0.6400	GMOS	0.67±0.05	115	G#7
8.360320	-19.33116	16.70±0.01	0.1470	GMOS	0.17±0.01	151	G#24
8.364630	-19.39061	19.73±0.06	0.4140	FORS2	0.44±0.06	149	#27
8.368750	-19.39239	20.71±0.11	0.4120	OSIRIS	0.58±0.11	146	P#20
8.369520	-19.35136	19.23±0.13	0.2900	FORS2	0.35±0.13	85	#11
8.371250	-19.34828	22.76±0.12	0.5350	OSIRIS	0.92±0.12	84	P#19
8.372214	-19.39001	20.50±0.09	0.4830	FORS2	0.47±0.09	132	#26
8.372987	-19.38060	21.97±0.74	0.4235	FORS2		103	#25
8.375833	-19.36253	20.56±0.10	0.4134	OSIRIS	0.39±0.10	60	P#17
8.376025	-19.33282	20.00±0.09	0.2190	FORS2	0.40±0.10	112	#23
8.376279	-19.35206	20.73±0.11	0.1605	GMOS	0.39±0.11	63	G#13
8.379091	-19.35232	18.18±0.03	0.1605	FORS2	0.10±0.03	54	#7
8.383750	-19.34083	21.93±0.21	0.1469	OSIRIS	0.47±0.21	74	P#16
8.384832	-19.38943	20.60±0.07	0.1360	FORS2	0.18±0.07	113	#24
8.386320	-19.33076	20.96±0.09	0.3520	GMOS	0.42±0.09	105	G#15
8.393923	-19.35252	19.42±0.04	0.2373	FORS2	0.20±0.04	24	#6
8.397430	-19.32274	19.62±0.08	0.3855	GMOS	0.46±0.08	132	G#18
8.402887	-19.38667	19.59±0.13	0.1085	FORS2	0.24±0.13	104	#9
8.408049	-19.31351	19.41±0.04	0.3330	GMOS	0.34±0.04	172	G#21
8.408534	-19.37380	19.84±0.08	0.6390	FORS2	0.58±0.08	74	#21
8.409522	-19.39235	20.04±0.18	0.5520	FORS2	0.37±0.18	132	#22
8.415103	-19.36052	19.88±0.07	0.3260	FORS2	0.44±0.07	74	#19
8.415633	-19.33170	19.23±0.12	0.2400	FORS2	0.37±0.12	125	#17
8.417479	-19.37740	17.88±0.05	0.2180	FORS2	0.16±0.05	105	#8
8.418285	-19.34955	21.41±0.07	0.3850	FORS2	0.24±0.07	92	#18
8.418388	-19.31421	21.05±0.16	0.4760	FORS2	0.49±0.16	183	#1
8.420417	-19.34903	20.28±0.08	0.5800	OSIRIS	0.53±0.08	99	P#7
8.420970	-19.31129	20.73±0.16	0.4750	GMOS	0.45±0.16	197	G#40
8.422495	-19.33668	18.10±0.03	0.1468	FORS2	0.10±0.03	128	#3
8.428500	-19.36273	19.40±0.10	0.2400	GMOS	0.29±0.10	120	G#30
8.429510	-19.33802	20.26±0.05	0.6550	GMOS	0.65±0.05	145	G#28
8.432358	-19.35128	17.57±0.02	0.1113	FORS2	0.12±0.02	136	#4
8.434077	-19.33986	20.65±0.12	0.5330	FORS2	0.30±0.12	155	#15
8.450750	-19.35922	20.44±0.12	0.4110	FORS2	0.36±0.12	195	#14

Table A2. Properties of the galaxies in the field of S2 0109+22. Columns are (1) right ascension in degrees, (2) declination is degrees, (3) SDSS z'-band magnitude, (4) redshift from multi-object spectroscopy, (5) instrument used to obtain the spectrum, (6) SDSS photometric redshift, (7) separation to blazar in arcseconds, and (8) source numbering shown in Fig. 4.

RA (deg)	DEC (deg)	z'_{AB} (mag)	SpecZ	Inst.	PhotoZ SDSS	$\Delta\theta$ (")	N
17.97224	22.71662	18.45±0.05	0.1835	FORS2	0.14±0.03	199	#29
17.98279	22.79652	18.51±0.04	0.330	FORS2	0.37±0.05	233	#13
17.98365	22.71332	18.02±0.02	0.1835	FORS2	0.19±0.03	174	#17
17.98917	22.75067	20.20±0.15	0.4901	GMOS	0.45±0.13	119	G#20
17.99043	22.78776	19.79±0.11	0.1840	FORS2	0.28±0.13	193	#12
17.99250	22.78633	20.63±0.16	0.6630	GMOS	0.54±0.10	185	G#29
17.99583	22.74864	19.78±0.10	0.7050	GMOS	0.52±0.07	95	G#19
17.99606	22.69881	17.72±0.03	0.0887	FORS2	0.10±0.04	188	#15
17.99691	22.76845	20.37±0.13	0.2665	FORS2	0.25±0.07	126	#9
17.99833	22.76058	21.30±0.29	0.8570	GMOS	0.88±0.22	104	G#27
18.00167	22.70736	19.87±0.12	0.3489	GMOS	0.40±0.10	152	G#30
18.00417	22.70047	20.68±0.20	0.4567	GMOS	0.35±0.13	171	G#31
18.00583	22.74936	20.58±0.12	0.6880	GMOS	0.92±0.04	63	G#38
18.00958	22.78503	20.94±0.24	0.1315	GMOS	0.30±0.08	155	G#23
18.01500	22.75117	21.86±0.39	0.6630	GMOS		40	G#36
18.01625	22.75006	20.15±0.11	0.2673	GMOS	0.38±0.11	34	G#9
18.01750	22.75922	20.46±0.13	0.3900	GMOS	0.38±0.07	59	G#10
18.02375	22.75386	19.36±0.08	0.2694	GMOS	0.36±0.07	35	G#6
18.02500	22.74794	17.43±0.02	0.2674	GMOS	0.32±0.02	14	G#3
18.02625	22.74583	20.35±0.11	0.2685	GMOS	0.24±0.13	9	G#5
18.02702	22.77615	18.25±0.05	0.1230	FORS2	0.06±0.04	116	#10
18.02750	22.74100	20.33±0.14	0.4950	GMOS	0.56±0.06	16	G#7
18.03042	22.74886	20.73±0.17	0.4915	GMOS		27	G#35
18.03154	22.78269	17.06±0.02	0.1230	FORS2	0.14±0.03	141	#11
18.03758	22.74753	18.13±0.03	0.2662	FORS2	0.25±0.03	46	#21
18.04417	22.73317	22.17±0.43	0.3345	GMOS		77	G#18
18.04583	22.75786	20.68±0.21	0.4950	GMOS	0.48±0.10	87	G#24
18.04792	22.73986	19.88±0.10	0.4930	GMOS	0.44±0.05	80	G#17
18.05326	22.77338	19.11±0.09	0.3500	FORS2	0.41±0.09	143	#25
18.05339	22.74637	18.31±0.03	0.1950	FORS2	0.24±0.04	97	#22
18.05458	22.75225	20.43±0.12	0.2685	GMOS		105	G#12
18.05865	22.74699	21.82±0.42	0.1860	GMOS	0.25±0.12	115	G#37
18.06000	22.78244	20.20±0.16	0.1867	GMOS	0.23±0.10	182	G#21
18.06671	22.74903	18.27±0.04	0.1855	FORS2	0.17±0.03	142	#23
18.06833	22.76264	20.70±0.28	0.5170	GMOS	0.37±0.06	161	G#16
18.06942	22.73990	18.00±0.04	0.1865	FORS2	0.18±0.04	151	#2
18.07092	22.76468	19.61±0.08	0.5155	FORS2	0.30±0.09	172	#8
18.07358	22.77303	18.69±0.05	0.4100	FORS2	0.38±0.03	194	#27